Hindawi
International Journal of Antennas and Propagation
Volume 2022, Article ID 2401586, 10 pages
https://doi.org/10.1155/2022/2401586

Research Article

Novel Technique of Gap Waveguide Cavity Resonator Sensor with High Resolution for Liquid Detection

Ammar Alhegazi,[1] Zahriladha Zakaria,[1] Noor Azwan Shairi,[1] Muhammad Ramlee Kamarudin,[2] Rammah A. Alahnomi,[1] AzieanMohd Azize,[1] Wan Haszerila Wan Hassan,[1] AmyrulAzuanMohd Bahar,[3] and Ahmed Jamal Abdullah Al-Gburi[1]

[1]*Microwave Research Group (MRG), Centre for Telecommunication Research & Innovation (CeTRI), Fakulti Kejuruteraan Elektronik dan Kejuruteraan Komputer (FKEKK), Universiti Teknikal Malaysia Melaka (UTeM), Hang Tuah Jaya, 76100, Durian Tunggal, Melaka, Malaysia*
[2]*Universiti Tun Hussein Onn Malaysia (UTHM), Batu Pahat 86400, Johor, Malaysia*
[3]*Intel Microelectronics, Bayan Lepas Free Zone, Penang 11900, Malaysia*

Correspondence should be addressed to Zahriladha Zakaria; zahriladha@utem.edu.my

Received 4 November 2021; Revised 10 April 2022; Accepted 11 April 2022; Published 28 April 2022

Academic Editor: Mustapha C E Yagoub

Copyright © 2022 Ammar Alhegazi et al. This is an open access article distributed under the Creative Commons Attribution License, which permits unrestricted use, distribution, and reproduction in any medium, provided the original work is properly cited.

This article proposes a novel microfluidic sensor designed with a highly accurate Q-factor for liquid detection. The proposed sensor is developed and implemented with a gap waveguide cavity resonator (GWCR) approach. The GWCR approach is formed from the two metallic plates denoted as upper and lower plates. These plates are separated by an array of metallic pins attached to the lower plate, leading to high electric field concentration. A microfluidic channel is created at the midpoint of each plate to place the holder of liquid under test (LUT). The GWCR provides a high electric field, which increases Q-factor and is shown to exhibit a significant improvement in sensitivity and linearity. To characterise and evaluate the dielectric properties of the fluid, the LUT is placed inside a hairlike glass, which passes through the microfluidic channels. The LUT perturbs the electric field distribution inside the GWCR, known as the perturbation principle. The relation between the LUT and the electric field changes the electric field behaviours in terms of resonant frequency, Q-factor, and transmission coefficient. The analysis of these changes in the electric field behaviours leads to identifying the dielectric properties of the LUT. The anonymous dielectric characteristics of LUT, permittivity, and loss tangent formulas are derived utilising the polynomial fitting approach. The measurement outcomes reveal that the stated sensor can measure the permittivity and loss tangent for both LUT samples, such as ethanol and methanol, at 6.1 GHz and 23.4°C.

1. Introduction

Developments in liquid characterisation techniques have been grown sharply in the last few years. Microwave sensors have been used to identify the dielectric properties of liquids, which is essential in industries such as those in quality control in food, chemical, pharmaceutical, biosensor, and biomedical industries [1–3].

Material characterisation using microwave resonant sensors is considered one of the most accurate ways to obtain dielectric properties. Liquid characterisation has been realised using a conventional waveguide, a dielectric and coaxial probe that provides high Q-factor and accuracy [4–7]. However, these traditional resonators are usually complex and expensive to manufacture [8, 9]. Thus, different methods have been used for liquid characterisation, such as planar resonators [10–13]. Planar resonator for petroleum oils characterisation was proposed in [14]. Substrate integrated waveguide (SIW) is another method for liquid detection [15–17]. These resonators are simple to design and

cheap to fabricate. However, usually, these resonators have low Q-factor, which limit their use in many critical applications. Some researchers tend to improve the Q-factor by using the metal waveguide method [18]. Most researchers used a cavity waveguide which is suitable for liquid sensing [19]. Some waveguide structures were designed at higher frequencies to miniaturise the size and characterise a nanoliter liquid sample [20–22]. However, these sensors required high frequency to operate. On the other hand, the complete microfluidic system of the waveguide sensors designed at lower frequencies is complex, large, and expensive to build [23]. A food security sensing system was proposed using a waveguide microwave imaging antenna applied for solid egg detection using a transmitting waveguide antenna (TWA) [24]. The suggested microwave sensors had a dimension of $30 \times 30\,\text{cm}^2$ and operated at frequency bands 7–13 GHz. Another study was conducted using waveguide antenna sensors for crack detection applications [25].

The gap waveguide (GW) terminology was initially launched in 2009 by Per Simon Kildal [26]. In the GW, the waves propagate between the parallel metal plates. The advantage of the GW compared to planar structures, coplanar waveguide (CPW), and substrate integrated waveguide (SIW) is that it has lower losses. The principle of operation of GW is based on two parallel plates' structure. Thus one plate acts as a perfect electric conductor (PEC), while the other plate acts as a perfect magnetic conductor (PMC) [26, 27]. A full electromagnetic wave propagates within the pins array boundaries. Hence the electric field is restricted along the pins array area, and this leads to avoiding the leakage of the electric field, which affects traditional technologies at higher frequencies [28]. There are four different configurations of the gap waveguide compositions, as displayed in Figure 1 [29, 30].

In the ridge gap waveguide presented in Figure 1(a), the field propagates through the metal ridge, while in the groove gap waveguide, shown in Figure 1(b), the field propagates through the groove between the parallel plates [28, 31]. The advantage of these two geometries is that they do not need any dielectric material between the plates and can be constructed by creating an array of metal pins under the plate [32]. In the microstrip gap waveguide displayed in Figure 1(c), the field propagates between the upper metal plate and the stripline [33]. In the microstrip gap waveguide exhibited in Figure 1(d), the field propagates along the strip with visas. Gap waveguide technology has gained researchers interest where it has been practised for antennas configuration as proposed in [34]. Moreover, the gap waveguide terminology has been used for millimetre wave applications such as couplers and filters [35]. In this paper, the pothole gap waveguide is selected to design the proposed sensor due to its advantages such as the simplicity, high electric field in the array pins area (pothole), and high Q-factor. These advantages make the groove gap waveguide suitable for liquid characterisation.

A new design of microwave sensors for liquid characterisation is introduced in this study. The novel design of the resonator sensor is formed and rested on the GWCR technique. The new sensor structure is constructed of two parallel plates and a pins array on the lower plate. It is worth mentioning that the materials of the proposed pins are all made from aluminium. The waves are propagating between the two parallel plates and restricted by the pins array. Thus, the new sensor affords a great electric field concentration in the pins array area, leading to a high Q-factor. In order to test the liquid, the LUT samples are installed in between the GWCR where the electric field will be as its maximum concentration utilising a glass capillary; therefore, a sensation phenomenon within the electric field and the LUT is acknowledged as perturbation theory. The stated resonator is verified through laboratory measurement and compared with other related literature studies. The corresponding equation between the permittivity and loss tangent is obtained based on the polynomial fitting approach. Lastly, the measurement outcomes indicated that the recommended sensor could detect ethanol and methanol efficiently.

2. Sensor Design and Configuration

The GWCR can be represented by two parallel plates and RLC equivalent circuit, as presented in Figure 2.

The variables of the equivalent circuit can be calculated according to the length of the plate (l), and the interval separating the two parallel plates (z) can be estimated using equations (1)–(4) [36]:

$$R = \frac{2R_s}{l}, \tag{1}$$

$$L = \frac{\mu z}{l}, \tag{2}$$

$$G = \frac{\omega \varepsilon', l}{z}, \tag{3}$$

$$C = \frac{\varepsilon' l}{z}. \tag{4}$$

The air filled the space between the two parallel plates; thus $\varepsilon' = 1, \varepsilon' = 0$ and $\mu = 1$.

The modelled sensor is proposed based on GW technology as suggested in [26]. The working mechanism of the GWCR depends on the upper and lower plates, and it is presented as follows: the upper plate serves as a perfect conductor to induce the magnetic conductor, which can also be defined as a perfect dielectric, whereas the lower plate works as a perfect conductor in terms of electric conductor. The artificial magnetic conductor (AMC) is produced by the surface of the pins array on the lower plate, which restricts the waves propagation within the pins array area. These waves are larger for more petite holes among the pins and the upper plate [28]. In the GWCR, distribution takes place in the region enclosed by the pins on all sides. The GWCR case supports a TE10 mode of the rectangular waveguide, as presented in Figure 3. The GWCR has less loss and high distribution of the electric field. Thus the GWCR is suitable for liquid characterisation.

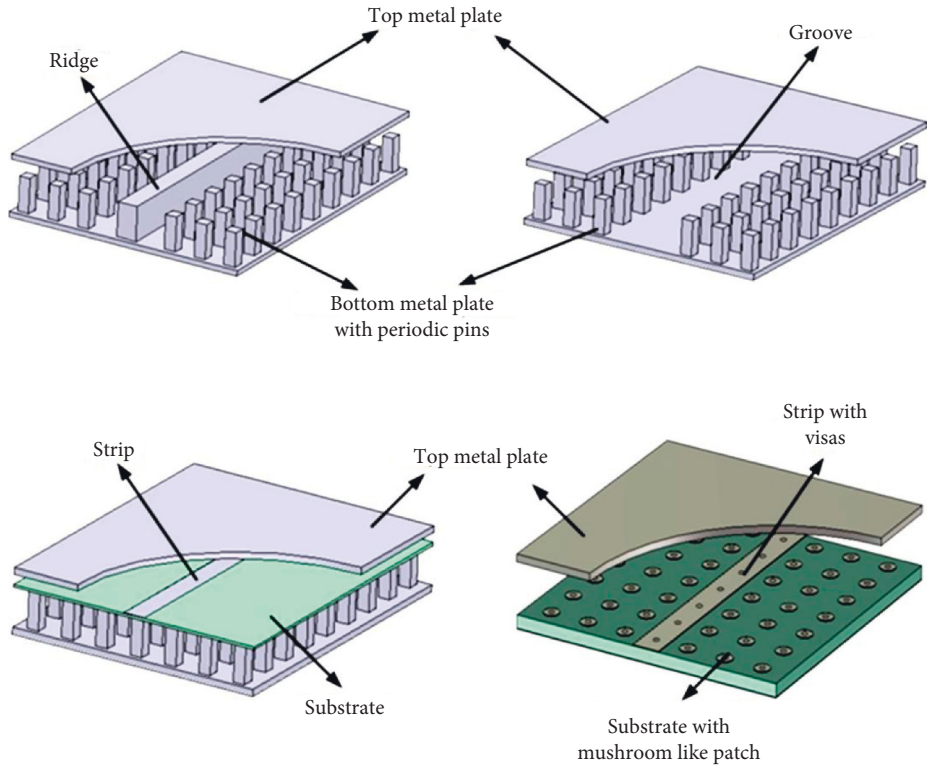

Figure 1: Proposed configurations. (a) Ridge GW. (b) Pothole GW. (c) Inverted-microstrip GW. (d) Microstrip-ridge GW [29].

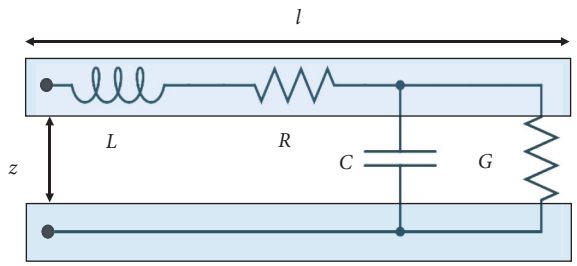

Figure 2: Geometrical diagram of the two parallel plates with the equivalent circuit.

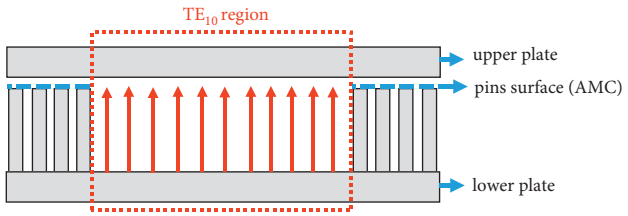

Figure 3: Geometrical diagram of the operating principle of the proposed GWCR.

Electric (E) and magnetic (H) fields of the GWCR can be described by Maxwell's equations [37, 38]:

$$\nabla \times E = -M - j\omega B, \tag{5}$$

where ω, B, and M are the radian frequency, magnetic flux density, and magnetic current density, respectively. The magnetic field can be expressed by

$$\nabla \times H = J + j\omega D, \tag{6}$$

where D and J are the electric flux density and the electric current density, respectively; the electric flux density and magnetic flux density can be expressed by

$$\begin{aligned} \nabla \cdot D &= \rho_e, \\ \nabla \cdot B &= \rho_m, \end{aligned} \tag{7}$$

where ρ_e and ρm are the electric and the magnetic charge density.

For TE modes, a natural boundary condition is described by the expression

$$E_\chi(y) = \overline{E}_0 \cos\left(\frac{y \cdot n\pi}{z}\right), \tag{8}$$

where n stands for a mode.

For harmonic TE mode wave is described by the expression:

$$\overline{E} = Z_0\left(\overline{H}_y i - \overline{H}_\chi j\right) = Z_0 \cdot n \times \overline{H}, \tag{9}$$

where Z_o is the wave impedance; at the same time, (5) can be expressed by

$$\nabla \times \overline{E} = -j\omega\mu\overline{H}. \tag{10}$$

In the microwave sensor design, the electric field is significantly considered to ensure a sufficient interaction between the LUT and the electric field of the resonator; thus, the sensor will be able to detect the dielectric characteristics of the material. The electronic concentration in the GWCR

can be measured by the Q-factor. Therefore, the high Q-factor reflects the high resolution [39]. The loaded Q-factor is equal to half unloaded Q-factor, where the unloaded Qu-factor (Qu) is calculated according to the 3 dB bandwidth (BW) and resonant frequency (f) using the following equation [40]:

$$Q_u = \frac{2f_o}{BW}. \tag{11}$$

The GWCR is studied and examined at 6.1 GHz, employing CST software. Figure 4 shows that the proposed structure consists of two parallel plates fed by two SMA connectors attached to the upper plate and a pins array on the lower plate. The pin sizes are standard of 1 mm^2 [31], and the gap between the upper cover of the pins and the top plate is found to be 1 mm, whereas the proportional thickness of the pin (h) is determined by [26]

$$h = \frac{\lambda}{4}, \tag{12}$$

where λ corresponds to the wavelength, which can be defined using the equation below:

$$h = \frac{c}{f_o}, \tag{13}$$

where c denotes the light speed, which is equivalent to 3×10^8 m/s, the estimated gaping among the pins is greater than 1.5 mm, and the height of each plate (thickness) is larger than 5 mm regarding the CNC device abilities. Table 1 presents the progressive values of the intended GWCR.

The waves are propagated between the two parallel plates and confined by the array pins from all directions to avoid the leakage of the electric field. Thus the electric field increases in the array pins area, as displayed in Figure 5. A glass capillary with a thickness of 0.21 mm is positioned in the centre of the cavity to characterise the liquid specimen, as illustrated in Figure 6. The electric field of the GWCR interacts with the LUT in the sensing area, and this manages to change the behaviour of the electric field due to the dielectric properties of the LUT. Hence it can be assumed that the relationship between the electric field and the dielectric properties is linear. The shifting of the resonance frequency depends on the reaction between the LUT and the electric field distribution of the sensor. The changes in the behaviour of the electric field are investigated and analysed to identify the dielectric properties of the LUT.

3. Results and Discussion

The proposed sensor's resonant frequency is controlled by changing the height of the pins on the lower plate, as illustrated in Figure 7. It can be remarked that the resonant frequency can be increased by reducing the height of the pins and vice versa. Therefore, when the pins' height is 12.7 mm, the resonant frequency occurs at 6.2824 GHz, while when the height of the pins is 18.7 mm, the resonant frequency rests at 5.9872 GHz.

The proposed sensor is fabricated using an aluminium alloy with an electric conductivity of $\sigma = 3.56 \times 107$. The simulation conditions of the modelled sensor are listed in Table 2. The measured outcomes reveal that the advanced sensor produces an unloaded Q-factor of 2650 at 6.0950 GHz. To validate the proposed sensor, the measurement is carried out for ethanol and methanol at room temperature of 23.4°C. Figure 8 presents the predicted and measured transmission coefficient (S21) of the designed resonator with/without LUT. From Figure 8, it is clear that there is a slight difference between simulation and measurement where the unloaded resonator for the measured one appears at 6.0950 GHz. This shifting in S21 is because of the fabrication tolerance, variation of substrate's dielectric constant, and the difference of the surrounding environment between the simulation and measurement. The noise that appears in the measured curve is due to external effects such as microwave signals that can affect the performance of the VNA [10].

In comparison, the simulated one seems at 6.1000 GHz, which is due to the manufacturing tolerance.

Based on the measurement results, the polynomial diagram is schemed based on the permittivity and frequency, as exhibited in Figure 9. The permittivity equation is obtained from the curve as follows:

$$\varepsilon' = 774.71f^2 - 9434.3f + 28722. \tag{14}$$

On the other hand, the permittivity equation can be extracted using matrix. By expressing the relationship between variables in the form of an equation:

$$\varepsilon' = a_2 f^2 + a_1 f + a_0. \tag{15}$$

Thus, the three data points in Figure 9 can be matched with the x and y coordinates, where the frequency matches with the x coordinate and the permittivity matches with the y coordinate; thus:

$$p(f) = a_0 + a_1 f + a_2 f^2 = \varepsilon'. \tag{16}$$

This gives a system of three equations and three unknowns as suggested:

$$\begin{bmatrix} 1 & 6.0475 & 36.5723 \\ 1 & 6.01 & 36.12 \\ 1 & 5.9675 & 35.611 \end{bmatrix} \begin{bmatrix} a_0 \\ a_1 \\ a_2 \end{bmatrix} = \begin{bmatrix} 0.96 \\ 4.46 \\ 11.06 \end{bmatrix}. \tag{17}$$

Using Cramer's rule to solve the linear system of equations to find the regression coefficients using the determinants of the square matrix, each of the coefficients may be determined using the following equation:

$$a_k = \frac{\det(M_i)}{\det(M)}, \tag{18}$$

where $k = N$-1, and $N = 3$ (data points). M_i is the matrix with the i^{th} column replaced with the column of the permittivity. For example:

$$M_0 = \begin{bmatrix} 0.96 & 6.0475 & 36.5723 \\ 4.46 & 6.01 & 36.12 \\ 11.06 & 5.9675 & 35.611 \end{bmatrix}. \tag{19}$$

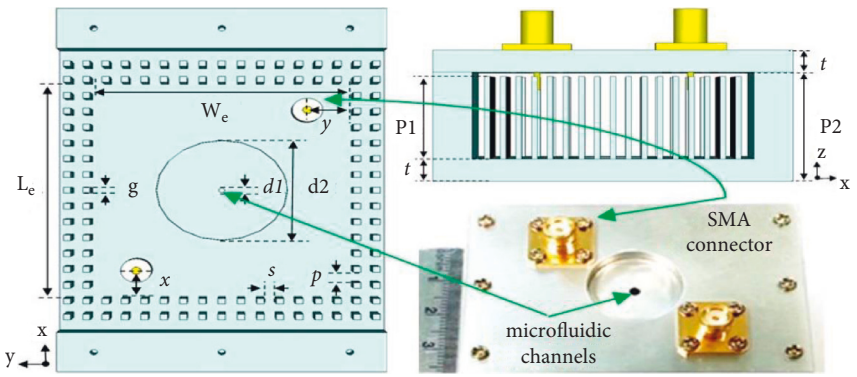

Figure 4: Structure of the proposed sensor.

Table 1: The selected values of the modelled sensor.

Variables	Values (mm)
L_e	38
W_e	35.4
g	1
d_1	1.7
y	6.3
P_2	21.75
d_2	18
x	5
s	1.6
p	1.8
P_1	15.73
z	16.74

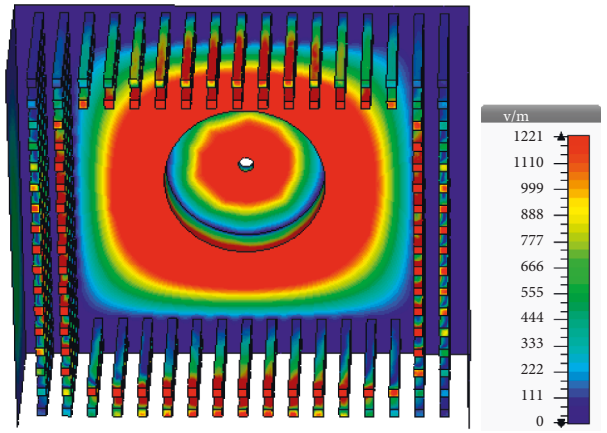

Figure 5: Predicated electric field (v/m) of the suggested sensor at 6.1 GHz.

Therefore, $\det(M_0) = -3.66787$. Thus, the polynomial coefficient is as follows:

$$a_0 = \frac{\det(M_0)}{\det(M)} = \frac{-3.66787}{-0.00013525} = 27119.1867. \quad (20)$$

The same goes with a_1 and a_2, and then the permittivity equation can be expressed as follows:

$$\varepsilon' = 730.1293 f^2 + 8899.6672 f + 27119.1867. \quad (21)$$

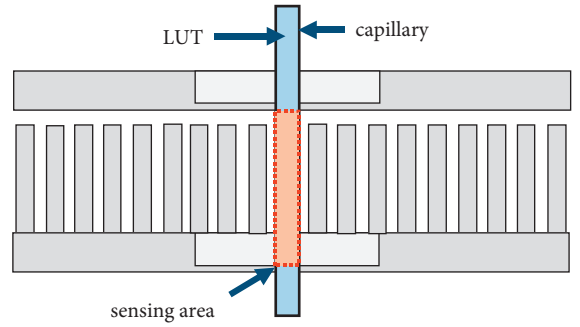

Figure 6: Geometrical diagram of the GWCR with WUT.

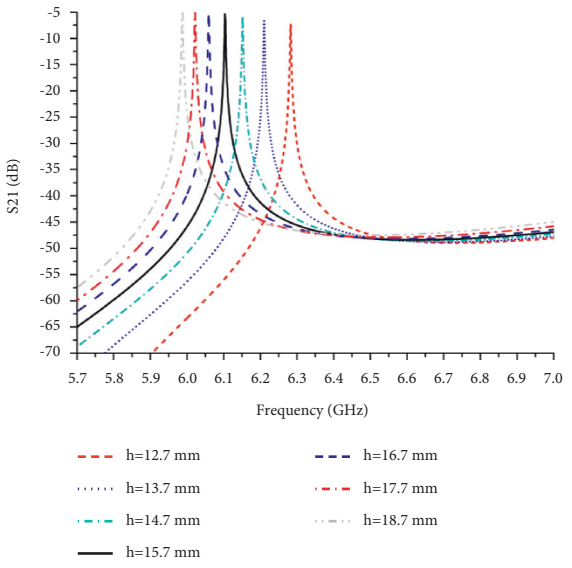

Figure 7: The predicated transmission coefficient of the proposed sensor with different values of h.

The number of the simulated data points in Figure 9 has been increased and then the figure has been constructed as shown in Figure 10.

$$\varepsilon' = 391.27 f^2 - 4784.4 f + 14626. \quad (22)$$

Figures 9 and 10 show the linearity of the frequency of resonance is decreasing by increasing the permittivity.

Table 2: Details of simulation conditions of the modelled sensor.

Dimensions unit	Frequency unit	Problem type	Solver	Mesh type	Parameters	Material type	Frequency (GHz)	Monitor	Impedance matching
mm	GHz	High frequency	Frequency domain	Tetrahedral	Fast model update	Normal	4–8	E-field	50 ohm

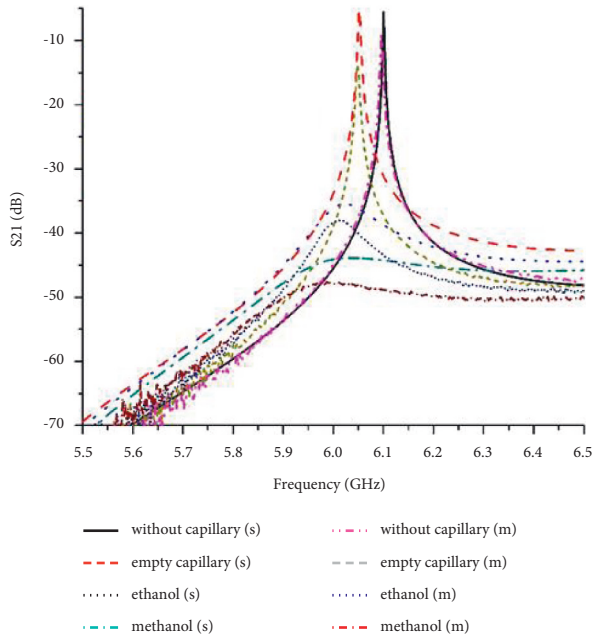

Figure 8: Predicated (s) and measured (m) S21 of the stated sensor with/without LUT.

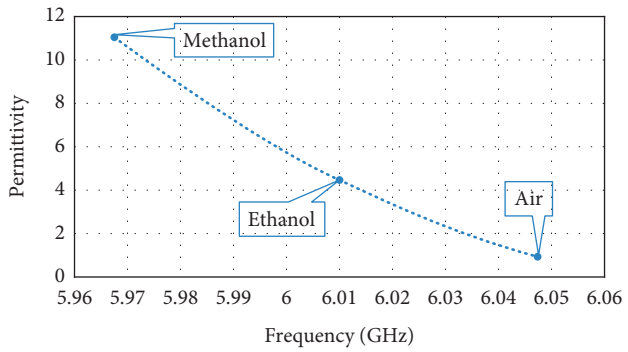

Figure 9: Measured polynomial fitting curve of the permittivity.

The measured polynomial fitting curve is plotted according to the loss tangent and the loaded Q-factor to obtain the loss tangent formula, as presented in Figure 11.

From Figure 11, the measured polynomial fitting curve of the loss tangent extracted equation is given by

$$\tan\delta = -4\times10^{-7}Q_L^2 - 0.0005Q_L + 0.9079. \quad (23)$$

By using matrix, the three data points in Figure 10 can be matched with the x and y coordinates, where the Q_L-factor matches with the x coordinate and the loss tangent matches with the y coordinate; thus:

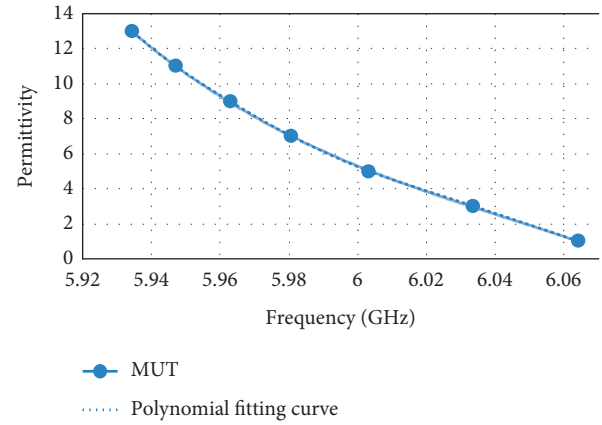

Figure 10: Simulated polynomial fitting curve of the permittivity.

Thus, the extracted equation is given by

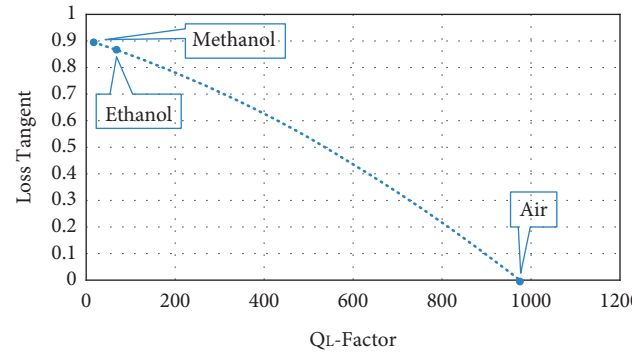

Figure 11: Measured polynomial fitting curve of loss tangent.

$$p(Q_L) = b_0 + b_1Q_L + b_2Q_L^2 = \tan\delta. \quad (24)$$

This gives a system of three equations and three unknowns as follows:

$$\begin{bmatrix} 1 & 972.85 & 946437.1225 \\ 1 & 66.815 & 4,464.244225 \\ 1 & 14.41 & 207.6481 \end{bmatrix}\begin{bmatrix} b_0 \\ b_1 \\ b_2 \end{bmatrix} = \begin{bmatrix} 0.043 \\ 0.873 \\ 0.901 \end{bmatrix}. \quad (25)$$

As discussed previously, the loss tangent equation can be expressed as follows:

$$\tan\delta = -3.983\times10^{-7}Q_L^2 - 0.0005Q_L + 0.9080. \quad (26)$$

The number of the simulated data points in Figure 11 has been increased and then the figure has been constructed as shown in Figure 12.

$$\tan\delta = -4\times10^{-16}\times Q_L^2 - 0.0037Q_L + 0.7995. \quad (27)$$

Figures 11 and 12 show the linearity of the loaded quality factor is decreasing sharply by increasing the loss tangent.

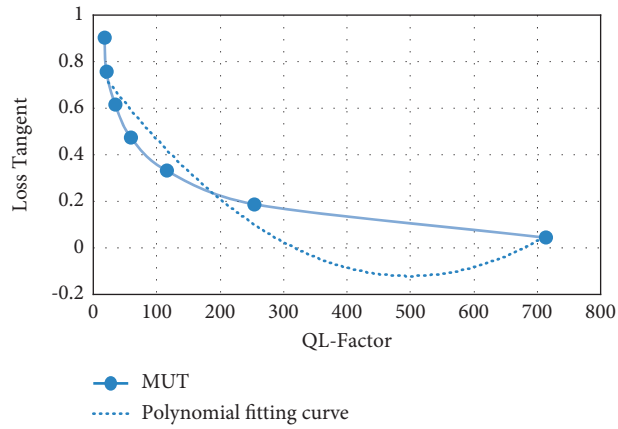

Figure 12: Simulated polynomial fitting curve of loss tangent. Thus, the simulated extracted equation of the loss tangent is given by

The number of the simulated data points in Figures 10 and 12 has been increased to 7 data points, with the permittivity of the MUT at range from 1 to 13 and the loss tangent of the MUT at range from 0.043 to 0.901. The linearity helps achieve higher effective sensitivity at various ranges of MUT. Therefore, the measured data points have been chosen to fit the parabolic functions for both permittivity (15) and tan delta (24) since the measured data points are reliable for usage in real life considering the real environmental conditions; thus the proposed sensor is suitable for liquid characterisation and a good candidate for industrial applications. However, increasing the data points in simulation produces a different polynomial fitting curve and equation from the polynomial fitting curve and equation of the measurement. This is due to the dielectric properties of the additional MUT in the simulation. The differences between simulations and measurements are also affected by the SMA connector losses in practice, as an ideal connector is modeled in simulations.

A comparison of the suggested sensor with the other detailed studies is depicted in Table 3.

From the previous results, it can be noted that, by placing the quartz capillary in the proposed sensor, the resonant frequency shifts to 6.0475 GHz due to the dielectric properties of the capillary. The empty capillary is filled with air, which means that the resonant frequency at 6.0475 GHz is considered for the dielectric properties of the air where the measured results show a permittivity of 0.9600 and loss tangent of 0.0430. The permittivity of the LUT causes a frequency shift into the lower frequencies, where the measured permittivity of the ethanol sample is 4.4600. The measured resonant frequency resonates at 6.0100 GHz, while the measured permittivity is 11.0600 for the methanol sample, and the measured resonant frequency rises at 5.9675 GHz. Also, it can be noted that the Q-factor decreases by increasing the loss tangent where the measured loss tangent for ethanol is 0.8730, the measured QL-factor is 66.8150, and when the loss tangent for methanol is 0.9010, the measured QL-factor is 14.4100. From Figure 8, it is clear that the transmission coefficient is decreasing by increasing the loss tangent where the transmission coefficient for ethanol is better than the transmission coefficient of the methanol. The relationship between the loss tangent, QL-factor, and transmission coefficient is illustrated in Figure 13.

From Table 3, there is a good matching among the proposed sensor and lately published works of literature for ethanol and methanol at 6.1000 GHz. Nevertheless, the slight change of the permittivity values at 6.1000 GHz is principally due to temperature variation. The relative permittivity of ethanol was 8.9100 and 24.0200 for methanol at 2.45 GHz and 30°C as proposed in [43]. Moreover, at 5 GHz and 25°C, the ethanol and methanol relative permittivity were 5.2200 and 13.2300, respectively, as detailed in [44].

As aforementioned above, the results confirmed that the stated sensor has a high Q-factor and miniature size, which means that it has high performance and low cost. In addition, the small size of the microwave sensor required only a small volume of the LUT to detect the dielectric characteristics.

To recognise the current work in context, the performance of the proposed GWCR sensor is compared with the other planar resonator sensors in the literature. Table 4 shows the performance attributes of several typical microwave sensors with different structures in terms of sensing material, sensor technique, resonance frequencies f_{res} (GHz), measured permittivity, and mean sensitivity. The experimental outcomes in the existing literature are offered for different ranges of permittivity; therefore, as a result of a fair comparison, the mean sensitivity values are calculated by the following expression:

$$\text{MeanSensitivity} = \left(\frac{f_{\varepsilon_{r2-}} f_{\varepsilon_{r1}}}{f_o\left(\varepsilon_{r_2} - \varepsilon_{r_1}\right)} \right) \times 100, \tag{28}$$

where $(f_{\varepsilon_{r2-}} f_{\varepsilon_{r1}})$ is the incremental frequency shift, (f_o) denotes to the resonant frequency (bare), and $(\varepsilon_{r_2} - \varepsilon_{r_1})$ indicates the permittivity shift. From the mentioned earlier formula we can conclude that the proposed GWCR sensor provides a good mean sensitivity when exposed to known

Table 3: Comparison of the stated sensor with lately published outcomes for both ethanol and methanol at 6.1 GHz.

LUT	Proposed sensor								Conventional sensors			
	ε'				tanδ				[41]		[42]	
	f (GHz)	Curve	Derivation	Error (%)	Q_L	Curve	Derivation	Error (%)	ε'	tanδ	ε'	tanδ
Air	6.0475	0.9600	0.9280	3.3000	972.8500	0.0430	0.0448	4	—	—	—	—
Ethanol	6.0100	4.4600	4.5866	2.7600	66.8150	0.8730	0.8730	0	4.5000	0.8700	—	—
Methanol	5.9675	11.0600	11.1000	0.3600	14.4100	0.9010	0.9010	0	—	—	11.1000	0.9000

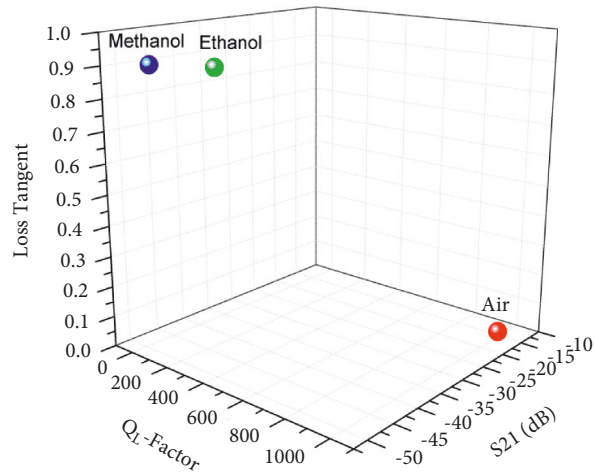

Figure 13: Relationship between the loss tangent, Q_L-factor, and transmission coefficient.

Table 4: Comparison of the finalised sensor with the current methods for liquid characterisation.

REF.	Sensor technique	$\mathbf{f_{res}}$ (GHZ)	Permittivity range studies	Mean sensitivity
[45]	MTM sensor	2.6	1–140	0.27
	OLR conventional	2.6	1–140	0.09
[46]	Loss-compensated SRR	1.156	1–80	-
[47]	Double SRR	1.86	2.2–22.5	0.07
[48]	SRR	1	1–45	0.002
[49]	$\lambda/2$	2.4	7.5–22	0.07
This work	GWCR	5.96	1–13	0.156

high-permittivity materials compared with the conventional highly sensitive sensor [45].

4. Conclusions

A novel design of a GWCR resonator sensor with a highly accurate Q-factor for liquid characterisation is introduced in this study. The main advantages of the proposed GWCR resonator are (1) more economical to build than the traditional metal waveguides and having (2) a lower loss with a higher Q-factor than microstrip structures. The modelled GWCR sensor used two liquid samples to validate the proposed sensor in the measurement setup: ethanol and methanol. The evaluated permittivity and loss tangent for ethanol and methanol at 6.1 GHz and temperature of 23.4°C have comparable results with the reference marks. The proposed GWCR shows the highest Q-factor compared to the recently published sensors. Besides, the GWCR sensor is shown to exhibit very high sensitivity and dynamic range versus the conventional MS sensors. Therefore, the finalised sensor is reliable, which makes it preferable for pharmaceutical applications.

Data Availability

All the data are included within the manuscript.

Conflicts of Interest

The authors declare that there are no conflicts of interest regarding the publication of this paper.

Acknowledgments

The authors would also like to thank Universiti Teknikal Malaysia Melaka (UTeM) for supporting this work under research Grants MTUNC/MC0011 and PJP/2019/FTKEE(2B)/S01654.

References

[1] A. P. Gregory and R. N. Clarke, "A review of RF and microwave techniques for dielectric measurements on polar liquids," *IEEE Transactions on Dielectrics and Electrical Insulation*, vol. 13, no. 4, pp. 727–743, 2006.

[2] S. N. Jha, K. Narsaiah, A. L. Basediya et al., "Measurement techniques and application of electrical properties for nondestructive quality evaluation of foods-a review," *Journal of Food Science & Technology*, vol. 48, no. 4, pp. 387–411, 2011.

[3] R. A. Alahnomi, Z. Zakaria, Z. M. Yussof et al., "Review of recent microwave planar resonator-based sensors," *Sensor Review*, vol. 2267, no. 21, pp. 1–38, 2021.

[4] U. Schwerthoeffer, R. Weigel, and D. Kissinger, "Microwave sensor for precise permittivity characterization of liquids used for aqueous glucose detection in medical applications," *Microw. Conf.*vol. 1, no. 4, pp. 1-2, 2014.

[5] T. Overview, *Keysight 85070E Dielectric Probe Kit 200 MHz to 50 GHz Swept High-Frequency Dielectric Measurements*, 2014.

[6] M. T. Jilani, M. Zaka, A. M. Khan, M. T. Khan, and S. M. Ali, "A brief review of measuring techniques for characterisation of dielectric materials," *Int. J. Inf. Technol. Electr. Eng.*vol. 1, no. 1, pp. 1–5, 2012.

[7] K. Y. You, "Materials characterization using microwave waveguide system," *Microwave Systems and Applications*, 2017.

[8] K. Shibata and M. Kobayashi, "Measurement of dielectric properties for thick ceramic film on an substrate at microwave frequencies by applying the mode-matchig method," in *Proceedings of the 2016 IEEE MTT-S International Conference on Numerical Electromagnetic and Multiphysics Modeling and Optimization (NEMO)*, pp. 8–11, Beijing, China, July 2016.

[9] A. Jamal Abdullah Al-Gburi, I. Ibrahim, Z. Zakaria, and A. Dheyaa Khaleel, "Bandwidth and gain enhancement of ultra-wideband monopole antenna using MEBG structure," *Journal of Engineering and Applied Sciences*, vol. 14, no. 10, pp. 3390–3393, 2019.

[10] A. A. Mohd Bahar, Z. Zakaria, S. R. Ab Rashid, a. a. M. Isa, and R. a. Alahnomi, "High-efficiency microwave planar resonator sensor based on bridge split ring topology," *IEEE Microwave and Wireless Components Letters*, vol. 27, no. 6, pp. 545–547, 2017.

[11] A. A. Mohd Bahar, Z. Zakaria, S. R. Ab Rashid, A. A. M. Isa, R. A. Alahnomi, and D. Tunggal, "Dielectric analysis of liquid solvents using microwave resonator sensor for high efficiency measurement," *Microwave and Optical Technology Letters*, vol. 59, no. 2, pp. 367–371, 2017.

[12] A. a. Abduljabar, D. J. Rowe, A. Porch, and D. a. Barrow, "Novel microwave microfluidic sensor using a microstrip split-ring resonator," *IEEE Transactions on Microwave Theory and Techniques*, vol. 62, no. 3, pp. 679–688, 2014.

[13] N. Rahman, Z. Zakaria, R. Rahim et al., "High quality factor using nested complementary split ring resonator for dielectric properties of solids sample," *Applied Computational Electromagnetics Society*, vol. 35, no. 10, pp. 1222–1227, 2020.

[14] S. Kulkarni and M. S. Joshi, "Design and analysis of shielded vertically stacked ring resonator as complex permittivity sensor for petroleum oils," *IEEE Transactions on Microwave Theory and Techniques*, vol. 63, no. 8, pp. 2411–2417, 2015.

[15] C. Fan Tong and F. Tong, "An SIW resonator sensor for liquid permittivity measurements at C band," *IEEE Microwave and Wireless Components Letters*, vol. 25, no. 11, pp. 751–753, 2015.

[16] A. Salim and S. Lim, "TM02 quarter-mode substrate-integrated waveguide resonator for dual detection of chemicals," *Sensors*, vol. 18, no. 6, p. 1964, 2018.

[17] Z. Wei, J. Huang, J. Li et al., "A high-sensitivity microfluidic sensor based on a substrate integrated waveguide Re-entrant cavity for complex permittivity measurement of liquids," *Sensors*, vol. 18, no. 11, pp. 4005–4017, 2018.

[18] H. Hamzah, A. Abduljabar, J. Lees, and A. Porch, "A compact microwave microfluidic sensor using a Re-entrant cavity," *Sensors*, vol. 18, no. 3, p. 910, 2018.

[19] P. Sharma, L. Lao, and G. Falcone, "A microwave cavity resonator sensor for water-in-oil measurements," *Sensors and Actuators B: Chemical*, vol. 262, pp. 200–210, 2018.

[20] N. Chudpooti, E. Silavwe, P. Akkaraekthalin, I. D. Robertson, N. Somjit, and I. D. Robertson, "Nano-fluidic millimeter-wave lab-on-a-waveguide sensor for liquid-mixture characterization," *IEEE Sensors Journal*, vol. 18, no. 1, pp. 157–164, 2018.

[21] V. Astley, K. Reichel, R. Mendis, and D. M. Mittleman, "Terahertz microfluidic sensing using a parallel-plate waveguide sensor," *Journal of Visualized Experiments*, vol. 66, pp. 1–5, 2012.

[22] X. Li, J. Song, and J. X. J. Zhang, "Design of terahertz metal-dielectric-metal waveguide with microfluidic sensing stub," *Optics Communications*, vol. 361, pp. 130–137, 2016.

[23] M. a. Al-Kizwini, S. R. Wylie, D. a. Al-Khafaji, and a. I. Al-Shamma'a, "The monitoring of the two phase flow-annular flow type regime using microwave sensor technique," *Measurement*, vol. 46, no. 1, pp. 45–51, 2013.

[24] T.-C. Tai, H.-W. Wu, C.-Y. Hung, and Y.-H. Wang, "Food security sensing system using a waveguide antenna microwave imaging through an example of an egg," *Sensors*, vol. 20, no. 3, p. 699, 2020.

[25] Q. Wang, K. Bi, Y. Hao et al., "High-sensitivity dielectric resonator-based waveguide sensor for crack detection on metallic surfaces," *IEEE Sensors Journal*, vol. 19, no. 14, pp. 5470–5474, 2019.

[26] P.-S. Kildal, E. Alfonso, A. Valero-Nogueira, and E. Rajo-Iglesias, "Local metamaterial-based waveguides in gaps between parallel metal plates," *IEEE Antennas and Wireless Propagation Letters*, vol. 8, pp. 84–87, 2009.

[27] A. J. A. Al-gburi, I. M. Ibrahim, Z. Zakaria, and M. K. Abdulhameed, "High gain of UWB planar antenna utilising FSS reflector for UWB applications," *Computers, Materials & Continua*, vol. 70, no. 1, 2022.

[28] E. Rajo-Iglesias and P.-S. Kildal, "Numerical studies of bandwidth of parallel-plate cut-off realised by a bed of nails, corrugations and mushroom-type electromagnetic bandgap for use in gap waveguides," *IET Microwaves, Antennas & Propagation*, vol. 5, no. 3, p. 282, 2011.

[29] R. Adawiyah, I. M. Ibrahim, A. J. A. Al-gburi, and Z. Zakaria, "Return loss improvement of radial LineSlot array antennas on closed ring resonator structure at 28GHz," *Przeglad Elektrotechniczny*, vol. 5, pp. 65–69, 2021.

[30] A. J. A. Al-Gburi, I. M. Ibrahim, Z. Zakaria, M. K. Abdulhameed, and T. Saeidi, "Enhancing gain for UWB antennas using FSS: a systematic review," *Mathematics*, vol. 9, no. 24, p. 3301, 2021, https://doi.org/10.3390/math9243301.

[31] A. K. Horestani and M. Shahabadi, "Balanced filter with wideband common-mode suppression in groove gap waveguide technology," *IEEE Microwave and Wireless Components Letters*, vol. 28, no. 2, pp. 132–134, 2018.

[32] M. G. Silveirinha, C. A. Fernandes, and J. R. Costa, "Electromagnetic characterisation of textured surfaces formed by

metallic pins," *IEEE Transactions on Antennas and Propagation*, vol. 56, no. 2, 2008.

[33] E. Pucci, A. U. Zaman, E. Rajo-Iglesias, and P. S. Kildal, "New low loss inverted microstrip line using gap waveguide technology for slot antenna applications," in *Proceedings of the Fifth European Conference on Antennas and Propagation*, pp. 979–982, EuCAP, Rome, Italy, April 2011.

[34] A. U. Zaman and P.-S. Kildal, "Slot antenna in ridge gap waveguide technology," in *Proceedings of the 2012 6th European Conference on Antennas and Propagation (EUCAP)*, pp. 3243-3244, Prague, Czech Republic, March 2012.

[35] E. Alfonso, A. U. Zaman, E. Pucci, and P.-S. Kildal, "Gap waveguide components for millimetre-wave systems: couplers, filters, antennas, MMIC," in *Proceedings of the International Symposium on Antennas and Propagation*, pp. 243–246, ISAP, Nagoya, Japan, November 2012.

[36] D. Pozar, *Microwave Engineering*, Fourth Edition, 2005.

[37] C. Balanis, *Advanced Engineering Electromagnetics*, p. 1989, John Wiley & Sons, 1989.

[38] R. F. Harrington and, *Time-Harmonic Electromagnetic Fields*, p. 2001, IEEE Press, 2001.

[39] K. Suwanna and S. Harnsoongnoen, "Non-contact active microwave sensor for glucose concentration measurement," *Journal of Physics: Conference Series*, vol. 1380, no. 1, p. 012026, 2019.

[40] A. Alhegazi, Z. Zakaria, R. A. Alahnomi, E. Ruslan, and S. R. A. Rashid, "Design of double ring resonator (DRR) for material properties measurement," in *Proceedings of the IEEE International Conference on Intelligent & Advanced Systems*, pp. 1–6, Kuala Lumpur, Malaysia, August 2016.

[41] M. M. Bajestan, A. A. Helmy, H. Hedayati, and K. Entesari, "A 0.62-10 GHz complex dielectric spectroscopy system in CMOS," *IEEE Transactions on Microwave Theory and Techniques*, vol. 62, no. 12, pp. 3522–3537, 2014.

[42] D. Misra, M. Chabbra, B. R. Epstein, M. Microtznik, and K. R. Foster, "Noninvasive electrical characterization of materials at microwave frequencies using an open-ended coaxial line: test of an improved calibration technique," *IEEE Transactions on Microwave Theory and Techniques*, vol. 38, no. 1, pp. 8–14, 1990.

[43] D. C. Campos, E. L. Dall'Oglio, P. T. De Sousa, L. G. Vasconcelos, and C. A. Kuhnen, "Investigation of dielectric properties of the reaction mixture during the acid-catalyzed transesterification of Brazil nut oil for biodiesel production," *Fuel*, PARTB, vol. 117, pp. 957–965, 2014.

[44] A. P. Gregory and R. N. Clarke, *Tables of the Complex Permittivity of Dielectric Reference Liquids at Frequencies up to 5 GHz*, 2012.

[45] M. Abdolrazzaghi, M. Daneshmand, and A. K. Iyer, "Strongly enhanced sensitivity in planar microwave sensors based on metamaterial coupling," *IEEE Transactions on Microwave Theory and Techniques*, vol. 66, pp. 1–13, 2018.

[46] M. Abdolrazzaghi, N. Katchinskiy, A. Y. Elezzabi, P. E. Light, and M. Daneshmand, "Noninvasive glucose sensing in aqueous solutions using an active split-ring resonator," *IEEE Sensors Journal*, vol. 21, no. 17, pp. 18742–18755, Sep. 2021.

[47] C. Yang Pu and Y. Pu, "A microstrip resonator with slotted ground plane for complex permittivity measurements of liquids," *IEEE Microwave and Wireless Components Letters*, vol. 18, no. 4, pp. 257–259, Apr. 2008.

[48] V. Sekar, W. J. Torke, S. Palermo, and K. Entesari, "A self-sustained microwave system for dielectric-constant measurement of lossy organic liquids," *IEEE Transactions on Microwave Theory and Techniques*, vol. 60, no. 5, pp. 1444–1455, May 2012.

[49] N. Wiwatcharagoses, K. Y. Park, J. A. Hejase, L. Williamson, and P. Chahal, "Microwave artificially structured periodic media microfluidic sensor," in *Proceedings of the IEEE 61st Electron. Compon. Technol. Conf. (ECTC)*, pp. 1889–1893, Lake Buena Vista, FL, USA, June 2011.